A&A 582, L3 (2015)
DOI: 10.1051/0004-6361/201527153

Astronomy & Astrophysics

Letter to the Editor

Hyperfine structure of the cyanomethyl radical (CH_2CN) in the L1544 prestellar core

C. Vastel[1,2], S. Yamamoto[3], B. Lefloch[4,5], and R. Bachiller[6]

[1] Université de Toulouse, UPS-OMP, IRAP, 31028 Toulouse, France
e-mail: charlotte.vastel@irap.omp.eu
[2] CNRS, IRAP, 9 Av. Colonel Roche, BP 44346, 31028 Toulouse Cedex 4, France
[3] Department of Physics, University of Tokyo, Bunkyo-ku, 113-0033 Tokyo, Japan
[4] Université de Grenoble Alpes, IPAG, 38000 Grenoble, France
[5] CNRS, IPAG, 38000 Grenoble, France
[6] Observatorio Astronómico Nacional (OAN, IGN), Calle Alfonso XII, 3, 28014 Madrid, Spain

Received 10 August 2015 / Accepted 16 September 2015

ABSTRACT

The L1544 prestellar core has been observed as part of the ASAI IRAM Large Program at 3 mm. These observations led to the detection of many complex molecules. In this Letter we report the detection of the cyanomethyl radical for the first time in a prototypical prestellar core, which is possible through the high sensitivity of the IRAM EMIR receiver. A complex structure in which we suspect the presence of the hyperfine transitions of the ortho and para forms is observed thanks to the high spectral resolution of ~50 kHz. We computed all transition frequencies and line intensities for all transitions including satellite hyperfine components for the ortho and para forms of CH_2CN at the frequencies observed by ASAI. We report the first detection of the fine and hyperfine structure of the ortho and para forms of the cyanomethyl radical at ~101 GHz, resolved in this cold dense core.

Key words. astrochemistry – line: identification – molecular data – radiative transfer

1. Introduction

The search for the cyanomethyl radical has been triggered by the detection of many unidentified transitions in the spectrum of the star-forming region SgrB2 (Cummins et al. 1986; Turner et al. 1975). CH_2CN has then been unambiguously detected a few years later for the first time in space towards the Sagittarius B2 star-forming region and the TMC-1 dark cloud by observation of rotational transitions by Irvine et al. (1988) using the spectroscopic laboratory measurements from Saito et al. (1988). Following these detections, the ground-state of the CH_2CN species has been characterised spectroscopically with the determination of the fine and hyperfine coupling constants of the molecule (Saito & Yamamoto 1997). Based on these calculations, Kaifu et al. (2004) identified many weaker lines in the TMC-1 dark cloud that were not reported in Irvine et al. (1988). Recent measurements have been performed by Ozeki et al. (2004) with the microwave spectrum of the cyanomethyl radical (CH_2CN) in its ground electronic state (X^2B_1) observed for the lowest three rotational transitions (N = 1–0 to 3–2) with a precise frequency accuracy of several kHz. As part of the IRAM-30 m Large Program ASAI[1] (Lefloch et al., in prep.), we have carried out a highly sensitive, unbiased spectral survey of the molecular emission of the L1544 prestellar core with the highest spectral resolution permitted by the IRAM 30 m FTS broad-band spectrometers.

In the present study we report on the detection of the CH_2CN molecule in the L1544 prestellar core, which was found to agree very well with our computations of the molecular fine and hyperfine structure components between 99 and 145 GHz. This is the first detection in a prototypical prestellar core and also the first detection of the hyperfine structure at this frequency.

[1] Astrochemical Surveys At Iram: http://www.oan.es/asai/

2. Observations

The observations were performed at the IRAM-30 m toward L1544 (α_{2000} = 05^{h}04^{m}17.21^s, δ_{2000} = 25°10′42.8″) using the broad-band receiver EMIR at 3 mm, connected to an FTS spectrometer in its 50 kHz resolution mode (see Vastel et al. 2014, for more details). Figures 1 and 2 show the detected transitions of the ortho and para forms of CH_2CN using the computed frequencies described in Sect. 3. The sensitivity of the observations is high enough that most of the hyperfine components are detected. We also detected several transitions of the para form in the range 101 520−101 535 MHz, although they are much weaker.

3. Calculation of line strengths

The hyperfine-resolved transition frequencies of CH_2CN are partly reported for transitions below the 60 GHz region by Ozeki et al. (2004). However, they are not available at higher frequencies. Then, we calculated them by using the molecular constants reported by Ozeki and collaborators. Since CH_2CN has a pair of identical hydrogen nuclei by symmetry, the spin states are classified into ortho and para states. As in the case of H_2, the para state has the total hydrogen nuclear spin of 0, while the ortho state has the total hydrogen nuclear spin of 1. The symmetry of the ground electronic state of CH_2CN is $^2B_1$, which is antisymmetric with respect to 180 degree rotation about the a-axis (the CCN axis). Hence, the nuclear spin state of I = 1 couples to rotational states with K_a = 0 (K_a is a projected quantum number

of the end-over-end rotation, N), whereas the nuclear spin state of $I = 0$ couples to rotational states with $K_a = 1$. This situation is opposite to the case of H_2CO, where the ortho and para states correspond to the $K_a = 1$ and $K_a = 0$ states, respectively.

To calculate line strengths of hyperfine-resolved rotational transitions, we used the following coupling scheme of angular momenta:
– J = N + S (S denotes the electron spin (=1/2))
– F_1 = J + I(N) (I(N) is the nuclear spin of the nitrogen nucleus (=1))
– F = F_1 + I(H) (I(H) is the nuclear spin of the hydrogen nucleus (=1))
for the ortho state, and there are six quantum numbers specifying each hyperfine level, F, F_1, J, N, K_a, K_c, where K_c is projection of N on the c axes. On the other hand, the coupling scheme is
– J = N + S
– F = J + I(N)
for the para state because I(H) = 0. Hence, there are five quantum numbers, F, J, N, K_a, and K_c.
With these basis sets, we set up the Hamiltonian matrices and obtained energy levels by direct diagonalisation of the matrices. We calculated the transition frequencies and the line strengths for a few low-N transitions with astronomical interests, as shown in Table 1. In calculations of line intensity, we rigorously considered mixing of wave functions used for the basis sets. Because of the relatively strong hyperfine interactions and the relatively weak spin-rotation interaction, the coupling scheme obtained above is only a poor approximation. Hence, considering the mixing of wave functions is indispensable for evaluating the line strengths.

4. Physical conditions and abundances

After computing the molecule frequencies, line intensities, and level energies, we implemented the results in the CASSIS[2] private database to perform a simple LTE modelling, considering both ortho and para states. L1544 is a prototypical prestellar core in the Taurus molecular cloud complex ($d \sim 140$ pc) on the verge of gravitational collapse (Caselli et al. 2012, and references within). The core is characterised by a low temperature (~7 K) and a high central density (higher than 10^6 cm^{-3}) in its centre. We note that the other detection of CH_2CN in a starless core was performed in the TMC-1 quiet dark cloud, which is characterised by a constant temperature of 10 K, and density of 2×10^4 cm^{-3}, and shows no signs of gravitational collapse. This stage represents an earlier phase of prestellar core formation. The high CO depletion observed in L1544 at the dust peak emission leads to a high deuterium fractionation (e.g. Vastel et al. 2006). Following the recent analysis by Vastel et al. (2014), we used a value of 10 K for the excitation temperature to estimate the column density for both forms. In Figs. 1 and 2, we present the results from the LTE radiative transfer modelling for the lowest energy levels transitions in which the lines have been detected. The spectra are perfectly reproduced using a column density of the ortho and para form of 3.5×10^{11} cm^{-2} for an excitation temperature of 10 K, using a full width at half maximum of 0.3 km s^{-1} at a systemic velocity of 7.25 km s^{-1}. The hyperfine structure for the ortho form is clearly identified. However, the hyperfine structure of the para form is not clearly detected, therefore we conclude that the observations at 99.7 and 101.5 GHz are compatible with an ortho-to-para (OPR) ratio of unity. The line at 101.53 GHz in Fig. 2 is detected through the blending of three nearby hyperfine structure transitions at 101.532089, 101.532038, and 101.532017 GHz (see Table 1).

An uncertainty on the column density and therefore abundance has to be considered using excitation temperatures between 5 and 15 K. Table 2 shows the column density for both ortho and para forms from a best-fit analysis, as well as the OPR.

[2] http://cassis.irap.omp.eu

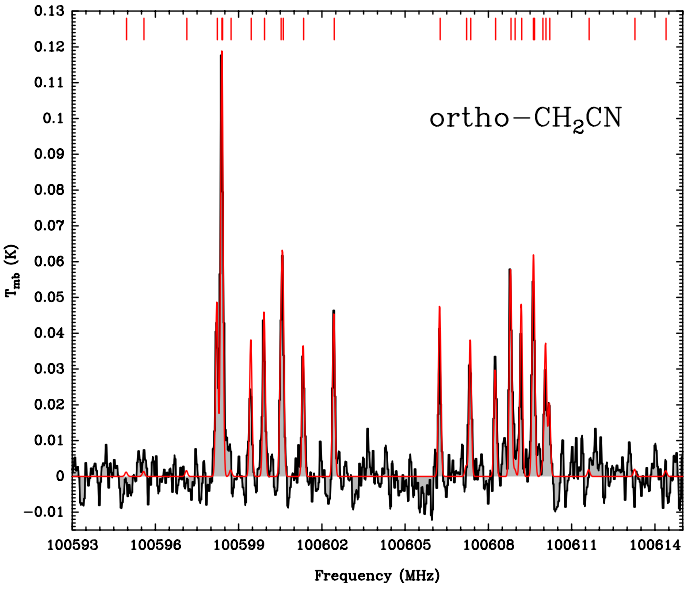

Fig. 1. Observation of the ortho-CH_2CN transitions around 100.6 GHz (in black) superposed with the LTE modelling in red. The upper red lines correspond to the frequencies in Table 1 shifted by 7.25 km s^{-1}.

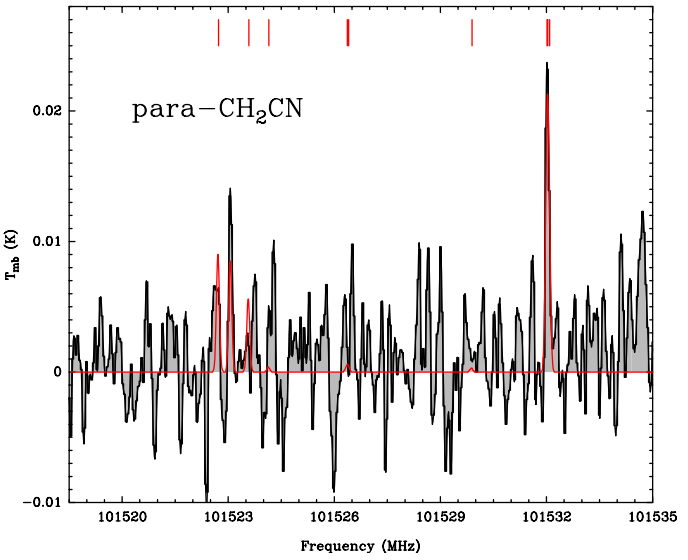

Fig. 2. Observation of the para-CH_2CN transitions around 101.5 GHz (in black) superposed with the LTE modelling in red assuming OPR = 1 with a best-fit column density from ortho-CH_2CN. The upper red lines correspond to the frequencies in Table 1 shifted by 7.25 km s^{-1}.

5. Chemical modelling

The dissociative recombination (DR) of the ion CH_3CNH^+ is the main pathway to form CH_2CN:

$$CH^+ \xrightarrow{H_2} CH_2^+ \xrightarrow{H_2} CH_3^+ \xrightarrow{HCN} CH_3CNH^+ \xrightarrow{e^-} CH_2CN, \quad (1)$$

Table 1. Spectroscopic parameters for the ortho $5_{0,5}$–$4_{0,4}$ and para $5_{1,4}$–$4_{1,3}$ transitions of the cyanomethyl radical.

$N'_{Ka'Kc'}$–$N''_{Ka''Kc''}$	J'	F'_1	F'	J''	F''_1	F''	Frequency (MHz)	A_{ij} (s^{-1})	E′ (cm^{-1})	E″ (cm^{-1})
					ortho					
$5_{0,5}$–$4_{0,4}$	5.5	6.5	7.5	4.5	5.5	6.5	100 598.4207	0.65982e-04	10.06610	6.71050
	5.5	6.5	6.5	4.5	5.5	6.5	100 607.2132	0.33993e-05	10.06640	6.71050
	5.5	6.5	6.5	4.5	5.5	5.5	100 600.6075	0.62365e-04	10.06640	6.71072
	5.5	6.5	5.5	4.5	5.5	5.5	100 617.0196	0.53295e-05	10.06694	6.71072
	5.5	6.5	5.5	4.5	5.5	4.5	100 602.4437	0.59911e-04	10.06694	6.71121
	5.5	5.5	6.5	4.5	5.5	6.5	100 587.9009	0.14738e-05	10.06575	6.71050
	5.5	5.5	6.5	4.5	4.5	5.5	100 598.3993	0.64507e-04	10.06575	6.71015
	5.5	5.5	5.5	4.5	5.5	5.5	100 592.8605	0.17122e-05	10.06614	6.71072
	5.5	5.5	5.5	4.5	4.5	5.5	100 609.9647	0.32683e-05	10.06614	6.71015
	5.5	5.5	5.5	4.5	4.5	4.5	100 599.9318	0.60682e-04	10.06614	6.71049
	5.5	5.5	4.5	4.5	5.5	4.5	100 597.1331	0.25876e-05	10.06677	6.71121
	5.5	5.5	4.5	4.5	4.5	4.5	100 618.7803	0.44696e-05	10.06677	6.71049
	5.5	5.5	4.5	4.5	4.5	3.5	100 601.3423	0.57963e-04	10.06677	6.71107
	5.5	4.5	5.5	4.5	4.5	5.5	100 592.2206	0.16293e-05	10.06555	6.71015
	5.5	4.5	5.5	4.5	3.5	4.5	100 598.2310	0.64339e-04	10.06555	6.70995
	5.5	4.5	4.5	4.5	4.5	4.5	100 595.5876	0.22087e-05	10.06599	6.71049
	5.5	4.5	4.5	4.5	3.5	4.5	100 611.6308	0.29660e-05	10.06599	6.70995
	5.5	4.5	4.5	4.5	3.5	3.5	100 599.4544	0.60597e-04	10.06599	6.71036
	5.5	4.5	3.5	4.5	4.5	3.5	100 598.7263	0.36535e-05	10.06668	6.71107
	5.5	4.5	3.5	4.5	3.5	3.5	100 620.0312	0.38912e-05	10.06668	6.71036
	5.5	4.5	3.5	4.5	3.5	2.5	100 600.5349	0.57819e-04	10.06668	6.71101
	4.5	5.5	6.5	3.5	4.5	5.5	100 608.8134	0.65705e-04	10.07028	6.71433
	4.5	5.5	5.5	3.5	4.5	5.5	100 594.9627	0.16207e-05	10.06982	6.71433
	4.5	5.5	5.5	3.5	4.5	4.5	100 606.2607	0.63612e-04	10.06982	6.71395
	4.5	5.5	4.5	4.5	5.5	4.5	100 635.9144	0.55255e-05	10.06806	6.71121
	4.5	5.5	4.5	3.5	4.5	3.5	100 610.0724	0.59231e-04	10.06806	6.71207
	4.5	4.5	5.5	3.5	4.5	5.5	100 614.4059	0.21198e-05	10.07047	6.71433
	4.5	4.5	5.5	3.5	3.5	4.5	100 609.1991	0.63566e-04	10.07047	6.71450
	4.5	4.5	4.5	3.5	4.5	4.5	100 608.9662	0.32846e-05	10.06991	6.71395
	4.5	4.5	4.5	3.5	3.5	3.5	100 607.3630	0.60468e-04	10.06991	6.71401
	4.5	4.5	3.5	4.5	4.5	3.5	100 648.8121	0.32736e-05	10.06835	6.71107
	4.5	4.5	3.5	3.5	4.5	3.5	100 618.7610	0.63549e-05	10.06835	6.71207
	4.5	4.5	3.5	3.5	3.5	2.5	100 609.6620	0.54699e-04	10.06835	6.71237
	4.5	3.5	4.5	3.5	3.5	4.5	100 617.1697	0.26790e-05	10.07073	6.71450
	4.5	3.5	4.5	3.5	2.5	3.5	100 609.6264	0.62973e-04	10.07073	6.71476
	4.5	3.5	3.5	3.5	3.5	3.5	100 613.2819	0.39214e-05	10.07011	6.71401
	4.5	3.5	3.5	3.5	2.5	2.5	100 608.2624	0.59445e-04	10.07011	6.71417
	4.5	3.5	2.5	4.5	3.5	2.5	100 659.6518	0.28291e-05	10.06865	6.71101
	4.5	3.5	2.5	3.5	3.5	2.5	100 618.6931	0.76819e-05	10.06865	6.71237
	4.5	3.5	2.5	3.5	2.5	1.5	100 610.2129	0.53783e-04	10.06865	6.71266
					para					
$5_{1,4}$–$4_{1,3}$	5.5		6.5	4.5		5.5	101 532.0886	0.65109e-04	19.32651	15.93977
	5.5		5.5	4.5		5.5	101 526.3684	0.20275e-05	19.32632	15.93977
	5.5		5.5	4.5		4.5	101 532.0377	0.63081e-04	19.32632	15.93958
	5.5		4.5	4.5		4.5	101 529.8965	0.24608e-05	19.32625	15.93958
	5.5		4.5	4.5		3.5	101 532.0169	0.62629e-04	19.32625	15.93951
	4.5		5.5	4.5		5.5	101 749.5061	0.15295e-05	19.33377	15.93977
	4.5		5.5	3.5		4.5	101 522.7268	0.63556e-04	19.33377	15.94733
	4.5		4.5	3.5		4.5	101 524.1474	0.32889e-05	19.33381	15.94733
	4.5		4.5	3.5		3.5	101 523.0744	0.60416e-04	19.33381	15.94737
	4.5		3.5	3.5		3.5	101 526.4048	0.40791e-05	19.33393	15.94737
	4.5		3.5	3.5		2.5	101 523.5827	0.59699e-04	19.33393	15.94746

and the photodissociation by interstellar UV photons is the main destruction process. We used the Nahoon[3] gas-phase chemical model (Wakelam et al. 2015), which computes the chemical evolution of a species as a function of time for a fixed temperature and density. The chemical network kida.uva.2014 contains 6992 unique chemical reactions and in total 7506 rate coefficients, and these reactions involve 489 different species. We do not pretend here to describe the situation with a self-consistent model, but to understand the influence of the C/O ratio needed to reproduce the observed CH_2CN. We ran different models with different initial parameters:

– Model 1: for the first step we adopted an elemental abundance for carbon of 5×10^{-5} and C/O = 0.5, a cosmic ionisation rate of 3×10^{-17} s^{-1}, a density of 2×10^4 cm^{-3}, and a temperature of 10 K and A_v = 10 and let the chemical

[3] http://kida.obs.u-bordeaux1.fr/models/

Table 2. Best-fit model for the ortho and para CH_2CN transitions using fixed excitation temperatures between 5 and 15 K.

T_{ex} (K)	N(o–CH_2CN) (cm^{-2})	N(p–CH_2CN) (cm^{-2})	OPR
5	2.6×10^{12}	2.2×10^{13}	0.1
8	5.5×10^{11}	1.0×10^{12}	0.6
10	3.5×10^{11}	3.8×10^{11}	0.9
12	2.3×10^{11}	2.1×10^{11}	1.1
15	1.7×10^{11}	1.1×10^{11}	1.5

composition evolve until steady state was reached. The abundances from this first step were then used as initial abundances for the second step, where the density is 4×10^6 cm^{-3} with an A_v of 30, as in Vastel et al. (2014) (Fig. 3, plain line).

- Model 2: same as model 1 with C/O = 0.7 (Fig. 3, dot-dashed line).
- Model 3: same as model 1 with C/O = 1 (Fig. 3, three-dots-dashed line).
- Model 4: same as model 1 with C/O = 1.2 (Fig. 3, dashed line).
- Model 5: only one step with an elemental abundance for carbon of 5×10^{-5} and C/O = 1, a cosmic ionisation rate of 3×10^{-17} s^{-1}, a density of 4×10^6 cm^{-3}, and a temperature of 10 K and $A_v = 30$ (Fig. 3, red line).
- Model 6: same as model 5 with C/O = 0.5 (Fig. 3, pink line).

The total column density of H_2 has been estimated in L1544 to be about 1.5×10^{23} cm^{-2}. If we consider that CH_2CN is emitted in the whole region, its abundance varies between 1.9×10^{-12} (at 15 K) and 1.6×10^{-10} (at 5 K). The chemical modelling is clearly dependant on the C/O ratio. When steady state is reached, the abundance is consistent with the computed abundance for an excitation temperature of 10–15 K for models 3 and 5. From the chemical reactions leading to the production of CH_2CN, we can also assume that the emission comes from the border of the L1544 core. Therefore, we must take into account a much lower H_2 column density. A column density of 5×10^{21} cm^{-2}, probing a region where CH_3OH is emitted (and most likely other COMs and C_3O; see Vastel et al. 2014), would lead to a higher abundance of 6×10^{-11} at 15 K. Even this higher value is significantly lower than the abundance found in the TMC-1 dark cloud ($\sim 10^{-9}$: Irvine et al. 1988 using the dipole moment calculated by Ozeki et al. 2004). It is linked to the chemical evolution from a typical dark cloud where carbon chain molecules are much more abundant than in the more evolved prestellar cores. CH_2CN and CH_3CN, which are assumed to form through the same chemical reactions (Eq. (1)), might then be good indicators of the chemical evolutionary stage of dark cloud cores (Vastel et al., in prep.). More precise computation need to be performed with a non-LTE modelling when the collision coefficients are available for temperatures below 20 K, and a study of the spatial extent of CH_2CN is needed to understand where it forms.

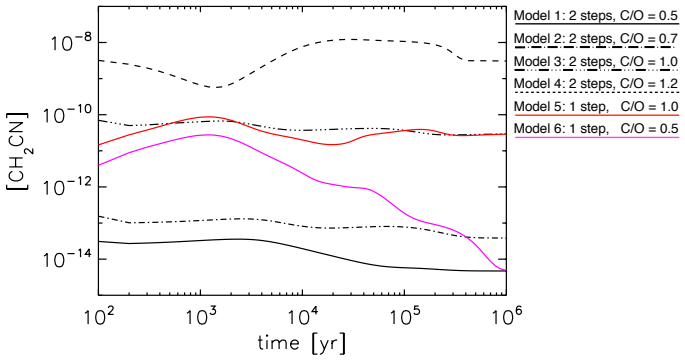

Fig. 3. Chemical modelling of the CH_2CN species using the most recent chemical network kida.uva.2014 (see text for the variation of parameters).

6. Conclusions

We conducted an unbiased spectral survey in the 3 mm band at the IRAM 30 m telescope within the Large Programme ASAI, towards the L1544 prestellar core. We detected the CH_2CN species at ~101 GHz with a complex structure that we attributed to an hyperfine structure. Following this detection, we computed the spectroscopic parameters for the lower energy transitions of the ortho and para transitions. This led to the first detection of the fine and hyperfine structure of the CH_2CN species in a prototypical prestellar core. It is the first detection of the hyperfine structure of the cyanomethyl radical at 3 mm, and the first detection of the hyperfine structure in its para form. We estimated the column density and abundance for both ortho and para CH_2CN and compared the observations with a gas-phase chemical modelling. We found that abundances between 10^{-12} and 10^{-11} are compatible with the observations for excitation temperatures between 10 and 15 K, much lower than the abundance found in the dark cloud TMC-1.

References

Caselli, P., Keto, E., Bergin, E. A., et al. 2012, ApJ, 759, 37
Cummins, S. E., Linke, R. A., & Thaddeus, P. 1986, ApJS, 60, 819
Irvine, W. M., Friberg, P., Hjalmarson, A. et al. 1988, ApJ, 334, 107
Kaifu, N., Ohishi, M., Kawaguchi, K., et al. 2004, PASJ, 56, 69
Ozeki, H., Hirao, T., Saito, S., & Yamamoto, S. 2004, ApJ, 617, 680
Saito, S., & Yamamoto, S. 1997, J. Chem. Phys., 107, 1732
Saito, S., Yamamoto, S., Irvine, W. M., Ziurys, L. M., et al. 1988, ApJ, 334, 113
Turner, B. E., Liszt, H. S., Kaifu, N., & Kisliakov, A. G. 1975, ApJ, 201, 149
Vastel, C., Caselli, P., Ceccarelli, C., et al. 2006, ApJ, 645, 1198
Vastel, C., Ceccarelli, C., Lefloch, B., & Bachiller, R. 2014, ApJ, 795, 2
Wakelam, V., Loison, J.-C., & Herbst, E. 2015, ApJS, 217, 20